Mathematical Biosciences and Engineering

http://www.aimspress.com/journal/MBE

MBE, 23(2): 421–448.
DOI: 10.3934/mbe.2026017
Received: 23 July 2025
Revised: 18 November 2025
Accepted: 27 November 2025
Published: 07 January 2026

Research article

EYE2HEART : A reduced mathematical model bridging cardiovascular and ocular hemodynamics

Lorenzo Sala[1,*], Mohamed Zaid[2], Faith Hughes[3], Marcela Szopos[4], Virginia H. Huxley[5], Alon Harris[6], Giovanna Guidoboni[3] and Sergey Lapin[7]

[1] Université Paris-Saclay, INRAE, MaIAGE, 78350, Jouy-en-Josas, France

[2] Foresite Healthcare LLC, Maryland Heights, Missouri 63043, USA

[3] Electrical and Computer Engineering, University of Maine, Maine, USA

[4] Université Paris Cité, CNRS, MAP5, F-75006 Paris, France

[5] Department of Medical Pharmacology and Physiology, School of Medicine, University of Missouri, Columbia, MO, United States

[6] Department of Ophthalmology, Icahn School of Medicine at Mount Sinai, New York City, NY, 10029, USA

[7] Department of Mathematics and Statistics, Program in Data Analytics, Washington State University Everett, Everett (WA), USA

* **Correspondence:** Email: lorenzo.sala@inrae.fr.

Abstract: The cardiovascular and ocular systems are intricately connected, with hemodynamic interactions playing a crucial role in both physiological regulation and pathological conditions. However, existing models often treat these systems separately, thus limiting the understanding of their interdependence. In this study, we present the EYE2HEART model, which is a novel closed-loop mathematical framework that integrates cardiovascular and ocular dynamics. Using an electrical-hydraulic analogy, the model describes the interactions between the heart and retinal circulation through a nonlinear system of ordinary differential equations. The model is tested against clinical and experimental data, thus demonstrating its ability to reproduce key cardiovascular parameters (*e.g.*, stroke volume, cardiac output) and ocular hemodynamics (*e.g.*, retinal blood flow). Additionally, we explore *in silico* the effects of intraocular pressure and left ventricular compliance on both local ocular and global systemic circulation, thus revealing critical dependencies between cardiovascular and ocular health. The results highlight the model's potential for studying cardiovascular diseases with ocular manifestations and support emerging research in oculomics by providing a mechanistic basis to interpret ocular biomarkers within a systemic context. This paves the way for patient-specific data integration and broader applications in personalized medicine.

Keywords: Cardiovascular system; ocular hemodynamics; oculomics; lumped-parameter model; ordinary differential equations; *in silico* experimentation; left ventricular compliance; intraocular pressure

1. Introduction

The ocular circulation is an integral component of the cardiovascular system, yet it possesses unique anatomical and physiological features that make it especially sensitive to systemic hemodynamic changes. Understanding this tight coupling is essential to study a wide range of physiological and pathological processes [1, 2]. The cardiovascular system regulates the systemic blood flow, which includes ocular perfusion, while the intraocular pressure (IOP) and retinal blood flow are critical to maintain ocular health. Studies have examined retinal vascular characteristics as indicators of cardiovascular health [3,4], and changes in the cardiovascular status are known to affect the retinal microvasculature [5]. This forms the foundation of *oculomics*, which is an emerging field that leverages ocular imaging to uncover systemic health conditions, particularly cardiovascular diseases [6, 7]. The retina, being a privileged access where microvasculature can be non-invasively visualized, serves as a powerful window into systemic physiology. Recent advancements, such as automated retinal photography and AI-based cardiovascular disease (CVD) risk assessment systems, have shown promise for non-invasive CVD risk evaluations, thereby presenting a more streamlined alternative to traditional clinical methods [8]. Additionally, the standardization and clinical use of retinal imaging biomarkers for CVD are becoming increasingly important in the effort to incorporate ocular data into cardiovascular risk assessments [9].

However, existing models often treat the cardiovascular and ocular systems as separate entities, thereby concentrating on either cardiac and vascular dynamics or isolated ocular physiology. This compartmentalized approach has led to a limited understanding of how the two systems interact. A more integrated view is necessary to capture their physiological interdependence. Current cardiovascular models typically do not account for the unique hemodynamic requirements of ocular perfusion, while ocular models frequently overlook the dynamic effects of cardiac function. The lack of a unified modeling framework has constrained the potential for accurate simulations of cardiovascular-ocular interactions across various physiological states. A recent study by Caddy and co-authors [10] attempted to model large-scale arterial hemodynamics from the heart to the eye under simulated microgravity conditions. Although this research represents a significant step in connecting cardiovascular and ocular dynamics, it primarily focuses on arterial circulation without incorporating closed-loop feedback mechanisms, which are vital to fully understand the complex interactions between these systems.

Previous work from our research group has developed theoretical models of both cardiovascular [11] and retinal networks [12], which were validated against clinical and experimental data. However, these models have remained isolated from each other. To address this limitation, we propose the development of a novel coupled Eye2Heart model. This model will serve as a virtual laboratory to investigate the integrated dynamics of cardiovascular and retinal blood circulation. The Eye2Heart framework is inherently multi-scale, thereby linking these two systems. Although the retina only receives a small fraction of cardiac output [13, 14], this flow is tightly coupled to the central hemodynamics and is critical for visual function. Therefore, even modest alterations in cardiac performance can have measurable

consequences at the ocular level, which makes the integration of macro- and micro-scale dynamics clinically relevant. The specific objectives of this research are twofold: (i) to develop and test a closed-loop heart-eye model that integrates both cardiovascular and ocular dynamics; and (ii) to simulate clinically relevant scenarios, such as variations in the IOP or changes in cardiac elastance, to explore the system behavior under diverse conditions. Through these efforts, we aim to provide a more comprehensive understanding of cardiovascular and ocular health, thus leading to new insights for clinical applications and therapeutic interventions. In doing so, our modeling framework contributes to the emerging field of oculomics by providing a mechanistic and quantitative approach to interpret ocular biomarkers in the context of the systemic cardiovascular function.

The remainder of the paper is as follows: Section 2 presents the mathematical framework, the assumptions underlying the Eye2Heart model, and the value of the parameter employed in the model for baseline simulations; Section 3 first details the testing process, thereby comparing our baseline results with experimental and clinical data, and then explores key simulation scenarios, including variations in the IOP and heart elastance; and finally, Section 4 discusses the implications of our findings, the limitations of the study, and directions for future research, including a preliminary local sensitivity analysis to quantify the influence of key parameters on systemic and ocular outputs.

2. Model and methods

This work presents a novel closed-loop mathematical model designed to capture the interplay between ocular and cardiovascular circulation, where variations in one system directly influence the other. The proposed coupling is formulated using a well-established set of ordinary differential equations (ODEs) derived under the assumption that hemodynamics can be represented by an electrical analog circuit. This modeling approach is widely used in the study of vascular dynamics and provides a robust foundation to simulate the bidirectional relationship between cardiovascular and ocular circulation. In this section, we describe the development, implementation, and parameterization of the closed-loop eye-heart model we designed, thereby emphasizing its potential to provide novel insights into the integrated function of these critical systems.

2.1. Closed-loop Eye2Heart *model*

Figure 1 illustrates the novel closed-loop Eye-Heart model, referred to as Eye2Heart hereafter. The system is built using an electrical circuit analogy, which is a widely adopted methodology in cardiovascular modeling [15]. In this framework, blood pressure, blood volume, and blood flow are represented by voltage, charge, and current, respectively.

Cardiovascular compartments, including blood vessels and heart ventricles, are represented using resistors (R) for vascular resistance, capacitors (C) for compliance, and inductors (L) for inertance. The heart is modeled using a time-varying elastance formulation, a standard approach in lumped-parameter cardiovascular modeling. By writing Kirchhoff laws for the nodes (conservation of current/flow rate) and for closed circuits (conservation of the voltage/pressure difference), the resulting mathematical model is a system of 23 ODEs that capture the dynamic interactions between the ocular and the cardiovascular circulatory systems. This structure provides a robust foundation to analyze and model the interconnected dynamics of these compartments. For clarity, the description is divided into three parts: the cardiovascular subsystem, the ocular subsystem, and the eye-heart coupling dynamics. All model

state variables and parameters are summarized in Tables 7 and 8 (in Appendix A), respectively, using physiologically descriptive symbols.

2.1.1. Cardiovascular System

The Eye2Heart model describes the cardiovascular system using a lumped-parameter formulation that is extended here to include the upper circulation that supplies the eye. This implementation builds upon the framework of Avanzolini et al. [16], with modifications introduced to enable coupling with the ocular circulation.

The left and right ventricular pressures are expressed as follows:

$$P_{\mathrm{LV}}(t) = U_L(t) + E_L(t)\, V_{\mathrm{LV}}(t), \tag{2.1}$$

$$P_{\mathrm{RV}}(t) = U_R(t) + E_R(t)\, V_{\mathrm{RV}}(t), \tag{2.2}$$

with the following time-dependent elastance and offset terms:

$$U_L(t) = U_{L0}\, a(t), \qquad E_L(t) = E_{LD} + E_{LS}\, a(t), \tag{2.3}$$

$$U_R(t) = U_{R0}\, a(t), \qquad E_R(t) = E_{RD} + E_{RS}\, a(t). \tag{2.4}$$

This formulation reproduces physiologically realistic pressure–volume dynamics during systole and diastole, thus supporting the generation of pulsatile flow patterns in the coupled system. We adopt the iso-volumic pressure generator formulation of Avanzolini et al. [16] to preserve the simplicity and parameter legacy of that model while focusing this study on the novelty of the systemic–ocular coupling. This choice allows us to reuse a well-established parameter set without re-estimating elastance parameters, thus limiting additional uncertainty.

The aortic pressure (P_{aorta}) and the right venous-atrial pressure (P_{vc}) are now interfaced with an *ad hoc* upper circulation module, which is designed to model blood flow to the ocular compartment and specifically to the retinal circulation.

To incorporate these dynamics, the original equations have been reformulated, thus ensuring the seamless integration of the new blood circulation pathway into the system. A key parameter, R_{body}, which represents the equivalent peripheral resistance of the body, has been updated to reflect the redistribution of blood volume toward the eye. In the original model, R_{body} was assigned a value of $6.75 \cdot 10^{-2}$ [mmHg $\cdot$ s $\cdot$ ml^{-1}]. In the revised eye-heart model, this parameter is adjusted to $6.93 \cdot 10^{-2}$ [mmHg $\cdot$ s $\cdot$ ml^{-1}], thus capturing the additional resistance introduced by the retinal blood flow dynamics.

Importantly, all other aspects of the cardiovascular system remain unchanged from the original model proposed by Avanzolini et al. [16]. These modifications solely focus on integrating the eye-specific circulation while preserving the original framework for the rest of the cardiovascular system. As such, the adopted strategy ensures consistency with the validated physiological dynamics described in the original model.

2.1.2. Ocular System

In the Eye2Heart model, the ocular subsystem incorporates a detailed representation of retinal circulation, divided into five main compartments: the central retinal artery (CRA), arterioles (art),

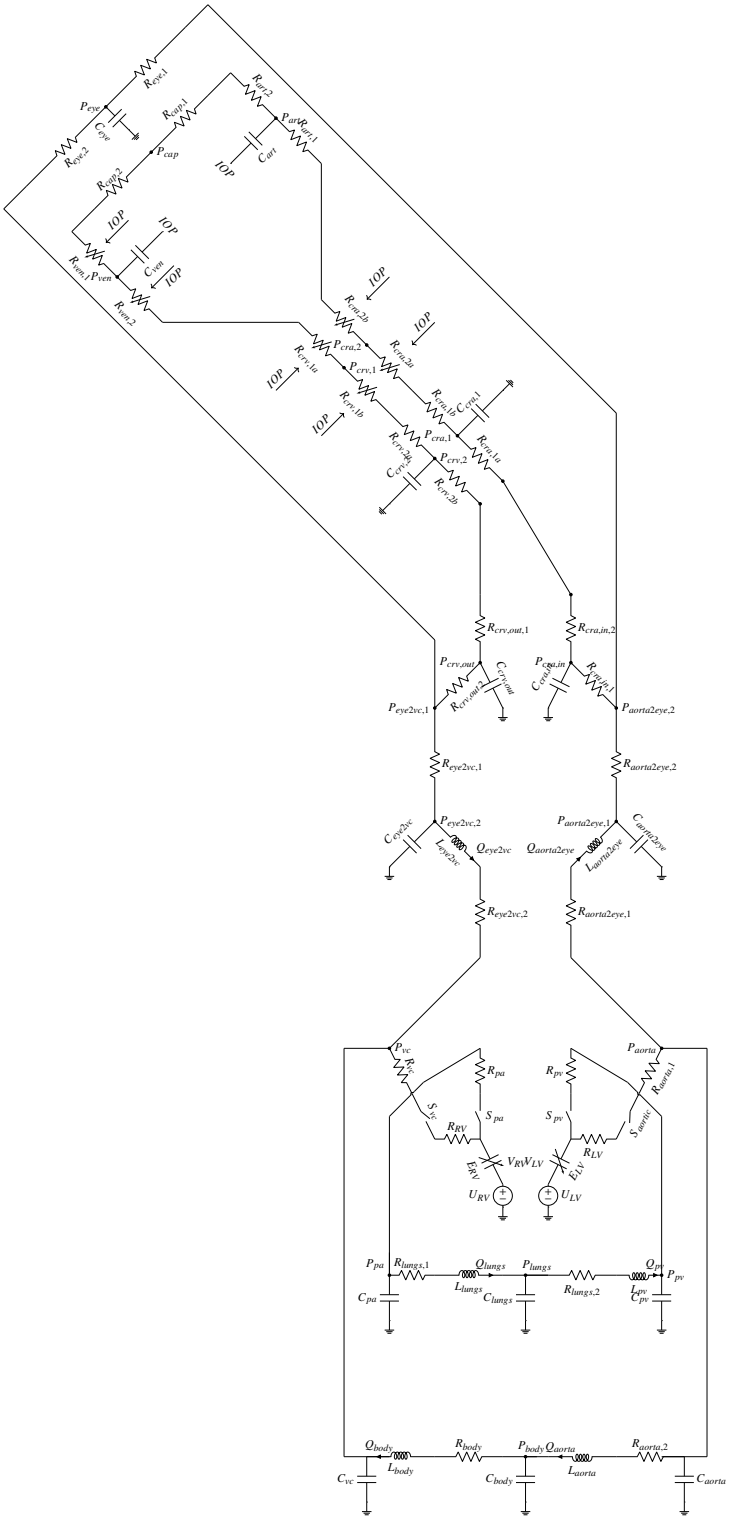

Figure 1. Model schematic of the EYE2HEART closed loop circuit. Variable resistances and capacitors are marked with arrows.

capillaries (cap), venules (ven), and the central retinal vein (CRV). Alphanumerical labels further distinguish between specific segments within each compartment. The blood flow within the retina is driven by a pressure difference between the inlet, $P_{cra,in}$, which is the blood pressure upstream of the CRA, and the outlet, $P_{crv,out}$, which is the pressure downstream of the CRV. At periodic steady state, the cycle-averaged CRA inflow equals the CRV outflow. In the reported values, small differences may appear because the CRA flow is measured pre-laminar and the CRV flow is measured post-laminar, with transient storage in the intervening compliances. We verified that no net fluid accumulation occurs over consecutive cycles. External pressures affect different parts of the retinal network: intraocular segments are exposed to the IOP, while retrobulbar segments behind the eye experience retrolaminar tissue pressure (RLTp). This combination of resistances and pressures provides a comprehensive blood flow model through the retinal vasculature. Following the notation in Figure 1, we can write the equations that describe the non-linear resistances. The resistances in the CRA, denoted as $R_{cra,2a}$ and $R_{cra,2b}$, are functions of the transmural pressure difference $\Delta P_{cra} = P_{cra,2} - \text{IOP}$, where $P_{cra,2}$ is the pressure in the CRA segment and the IOP is the intraocular pressure (see Figure 1).

They are modeled as follows:

$$R_{\text{cra},i} = \frac{1}{k_{0_{\text{cra},i}}} \left(1 + \frac{\Delta P_{\text{cra}}}{K_{p_{\text{cra},i}}\, K_{l_{\text{cra},i}}}\right)^{-4}, \quad i \in \{2a, 2b\}. \tag{2.5a}$$

The venous segment includes two nonlinear components: $R_{\text{ven},1}$ and $R_{\text{ven},2}$ for the retinal venules, and $R_{\text{crv},1a}$ and $R_{\text{crv},1b}$ for the CRV. The nonlinearity arises due to the transmural pressure differences, which are defined as follows:

$$\Delta P_{\text{ven}} = P_{\text{ven}} - \text{IOP}, \qquad \Delta P_{\text{crv}} = P_{\text{crv},1} - \text{IOP}, \text{ respectively}$$

For the venular segments ($i \in \{1, 2\}$), the resistance is defined as follows:

$$R_{\text{ven},i} = \begin{cases} \dfrac{1}{k_{0_{\text{ven},i}}} \left(1 + \dfrac{\Delta P_{\text{ven}}}{K_{p_{\text{ven,i}}}\, K_{l_{\text{ven,i}}}}\right)^{-4}, & \text{if } \Delta P_{\text{ven}} \geq 0, \\ \dfrac{1}{k_{0_{\text{ven},i}}} \left(1 - \dfrac{\Delta P_{\text{ven}}}{K_{p_{\text{ven,i}}}}\right)^{4/3}, & \text{if } \Delta P_{\text{ven}} < 0. \end{cases} \tag{2.5b}$$

For the CRV segments ($j \in \{1a, 1b\}$), the resistances are defined as follows:

$$R_{\text{crv},i} = \begin{cases} \dfrac{1}{k_{0_{\text{crv},i}}} \left(1 + \dfrac{\Delta P_{\text{crv}}}{K_{p_{\text{crv,i}}}\, K_{l_{\text{crv,i}}}}\right)^{-4}, & \text{if } \Delta P_{\text{crv}} \geq 0, \\ \dfrac{1}{k_{0_{\text{crv},i}}} \left(1 - \dfrac{\Delta P_{\text{crv}}}{K_{p_{\text{crv,i}}}}\right)^{4/3}, & \text{if } \Delta P_{\text{crv}} < 0. \end{cases} \tag{2.5c}$$

These nonlinear components are fundamental to capture the dynamic interplay between pressure, flow, and vessel mechanics in the coupled eye–heart system.

In the Eye2Heart model, the ocular subsystem incorporates the retinal circulation as described by Guidoboni et al. [12]. This framework, which includes vascular resistance, compliance, and blood flow dynamics across the CRA, arterioles, capillaries, venules, and the CRV, is adopted without modification to preserve consistency with validated physiological and experimental observations of retinal

hemodynamics. Moreover, building upon the base model of the retinal circulation, we further introduce an additional parallel circuit, referred to as the eye branch, which represents the blood flow directed toward non-retinal structures. Although the term "eye branch" can be seen as a simplification, it is intended to encompass all ocular vascular beds outside the retina, such as the choroid and ciliary body. This extension enables the model to capture the broader ocular circulation, thereby accounting for the distinct hemodynamic properties and functional roles of these non-retinal structures. By incorporating the eye branch, the model provides a more comprehensive representation of blood flow within the eye and accounts for flow redistribution mechanisms under conditions of elevated external pressure.

2.1.3. Eye-Heart Coupling

The EYE2HEART model incorporates a dedicated eye–heart coupling component that captures the dynamics of blood circulation between the heart and a single eye. The systemic cardiac output is partitioned into two branches: one directed to the ocular circulation and the other representing the rest of the body, including the brain and peripheral tissues. This separation enables a targeted analysis of the ocular hemodynamics without compromising the systemic integrity.

The resting cardiac output in healthy adults is about 5 L/min [13], while the ophthalmic artery flow is reported as roughly 10 mL/min per eye [14], which only corresponds to ∼0.2–0.3% of the cardiac output per eye (∼0.4–0.6% for both eyes). Despite this small fraction, its tight coupling to central hemodynamics makes even small systemic variations detectable at the microvascular level. This macro-to-micro integration is a key novelty of the model.

The direct connection between the heart and the eye is described using an aorta-to-eye and eye-to-vena cava equivalent circuit, which is represented by resistive, capacitive, and inductive elements. These elements collectively simulate the vascular resistance, compliance, and volumetric blood flow within the pathway from the aorta to the ocular circulation and back to the venous system. By calibrating the R, C, and L parameters, the model captures the distinctive hemodynamic properties of the eye, including its dependence on the systemic blood pressure and flow rates which originate from the heart.

This simplification enhances the computational efficiency and allows for a detailed exploration of the interplay of cardiovascular and ocular systems. It provides a robust framework to investigate eye-specific circulatory phenomena, such as retinal blood flow regulation and pressure-induced vascular changes. A detailed formulation of the full set of model equations is provided in Appendix C.

2.2. Solution strategy and model calibration

Whenever possible, we adopted parameter values reported in prior studies, as summarized in Appendix B. Parameters introduced in this work, particularly those which govern the coupling between cardiovascular and ocular circulation, were obtained through a calibration strategy based on steady-state physiological targets. Specifically, we used literature data on retinal flows reported by Dorner et al. [17] as reference values. To calibrate the coupling parameters, we considered the reduced circuit with only resistive components and applied Kirchhoff's laws to compute the parameter values offline. Then, these offline estimates were directly adopted in the coupled model without further tuning. To check the parameter consistency, we verified that the steady-state solutions produced physiological values when literature-based flows and pressures were imposed. A full verification of the complete model against literature data is presented in the results section.

The initial conditions for state variables were taken from published references for cardiovascular and ocular compartments [12, 16]. For the coupling compartments, the pressures and flows were set by running preliminary simulations until a periodic steady state was achieved. Appendix A summarizes the state variables and corresponding initial conditions.

In terms of the numerical strategy, the Eye2Heart mathematical model was implemented in MATLAB and solved using the stiff solver ODE15s [18], which is a variable-step, variable-order solver designed to efficiently solve stiff ODEs. ODE15s was chosen to solve the system of ODEs due to its ability to efficiently handle the strong nonlinear components of the model, thus ensuring stable and accurate numerical solutions. The solver was configured with a relative tolerance of 10^{-13} and an absolute tolerance 10^{-5}, thus ensuring a high numerical precision. A fixed time step of 0.001 s was used throughout the simulations. Transient dynamics at the beginning of the simulation were discarded to ensure analysis was performed under periodic steady state. Although only a small fraction of cardiac output is directed to the eye, this configuration provides stable and accurate solutions across both the macro- and micro-scale compartments, thus preserving the mass balance and pressure–flow consistency.

3. Simulation results of the Eye2Heart model

3.1. Model simulations against clinical ranges

The calibration of model parameters was based on values reported in the literature and adjusted to match steady-state physiological targets in simplified settings. These parameters had been previously validated in separate cardiovascular and ocular models, but not within a fully coupled framework where the closed-loop feedback between the two systems can emerge. For this reason, we simulate the complete Eye2Heart model, thereby comparing its results against clinical ranges and assessing whether the coupled dynamics consistently reproduce physiological values across systemic and ocular compartments. The following key parameters are computed and contrasted with clinical literature:

- End-Diastolic Volume (EDV): Maximum ventricular volume during the cardiac cycle.
- End-Systolic Volume (ESV): Minimum ventricular volume during the cardiac cycle.
- Ventricular End-Diastolic Pressure (VEDP): pressure in the ventricle at the end of diastole, representing the preload required to achieve the desired cardiac output.
- Stroke Volume (SV): $SV = EDV - ESV$, representing the amount of blood ejected per beat.
- Cardiac Output (CO): $CO = HR \times \dfrac{SV}{1000}$, measuring total blood flow per minute, where HR is the heart rate.
- Ejection Fraction (EF): $EF = 100 \times \dfrac{SV}{EDV}$, quantifying ventricular efficiency as the percentage of blood ejected during each beat.
- End-Systolic Elastance (E_{es}): slope of the end-systolic pressure-volume relationship.
- Arterial Elastance (E_a): estimate of aortic input impedance.
- Central Systolic and Diastolic Pressures (SP/DP).
- Right Atrial Pressure (P_{ra}).

Table 1 presents a comparison between the model predictions and clinical reference values, thereby considering these quantitative indicators.

Table 1. Cardiovascular physiology indicators, left and right ventricles: Comparison between clinical ranges from literature and simulation results from the present work.

Parameter	Unit	Clinical Ranges from literature		Present work	
		Left Ventricle	*Right Ventricle*	*Left Ventricle*	*Right Ventricle*
End-Systolic Volume (ESV)	[ml]	47 (27,68) [19] 35 ±13 [21] 30 ± 12 [22]	50 (22,78) [20] 43 ± 19 [21] 50-100 [23]	42.59	43.81
End-Diastolic Volume (EDV)	[ml]	142 (102,183) [19] 108 ±27 [21] 109 ± 27 [22]	144 (98,190) [20] 115 ± 31 [21] 100 - 160 [23]	112.76	115.25
Ventricular End-Diastolic Pressure (VEDP)	[mmHg]	8.3 ±3.6 [24]	0-8 [25]	6.923	1.846
Stroke Volume (SV)	[ml/beat]	95 (67, 123) [19] 60 - 100 [23] 81 ± 18 [26] 78 ± 20 [22]	94 (64, 124) [20] 60-100 [23]	70.18	71.45
Cardiac Output (CO)	[l/min]	4-8 [23] 5.524 ± 1.488 [26] 4.8 ± 1.3 [22]	4-8 [23]	5.26	5.36
Ejection Fraction (EF)	[%]	67 (58, 76) [19] 72 ± 7 [22]	66 (54, 78) [20] 40 - 60 [23]	62.32	61.99
End-Systolic Elastance (E_{es})	[mmHg/ml]	1.74 [27]	0.7 ± 0.2 [28]	1.03	0.32
Arterial Elastance (E_a)	[mmHg/ml]	1.2 [27]	0.5 ± 0.2 [28]	1.65	0.52
Central Systolic Pressure (SP)	[mmHg]	124.1 ± 11.1 [29]		125.7	
Central Diastolic Pressure (DP)	[mmHg]	77.5 ± 7.1 [29]		72.7	
Right Atrial Pressure (P_{ra})	[mmHg]	3 ± 2 [30]		3.78	

The model predictions for key cardiovascular biomarkers, including ventricular volumes, stroke volume (SV), cardiac output (CO), and ejection fraction (EF), show good agreement with clinical val-

ues. EDV and ESV for both ventricles fall within expected ranges, with only slight underestimations, likely due to simplifications in compliance or pressure–volume assumptions.

The SV is well reproduced within the physiological limits, and the CO remains in the expected 4–8 L/min range, thus confirming the model's ability to capture fundamental cardiac dynamics. The EF is slightly lower than some reports but within a reasonable range, thus suggesting possible refinements in contractility or vascular resistance could improve the accuracy. Overall, the model provides a robust framework for cardiac function.

The predicted end-systolic elastances (E_{es}) are 1.03 mmHg/ml (LV) and 0.32 mmHg/ml (RV), which are slightly higher than values in [27,28]. This difference may stem from simplified elastance dynamics and the lack of inter-individual variability, particularly for the LV.

For the arterial elastance (E_a), the LV predictions are modestly higher than clinical values [27], while the RV predictions align well. This is consistent with the slightly reduced EF observed, since EF = SV/EDV: higher elastance lowers the EDV while preserving the SV, which leads to a reduced EF. Despite this deviation, all simulated indices remain physiological.

The predicted systolic and diastolic pressures (125.7/72.7 mmHg) match the clinical values, and the right atrial pressure (3.78 mmHg) lies within the 3 ± 2 mmHg range [30], thus supporting the model's ability to capture the venous pressure.

Physiological consistency is further illustrated by the Wiggers diagram (Figure 2) and pressure–volume loop (Figure 3), which reproduce typical phases of ventricular function, including isovolumetric contraction and relaxation [31].

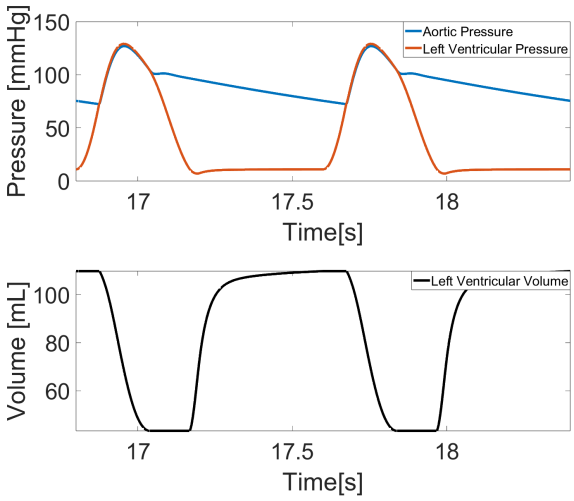

Figure 2. Wiggers diagram simulated *via* the Eye2Heart model.

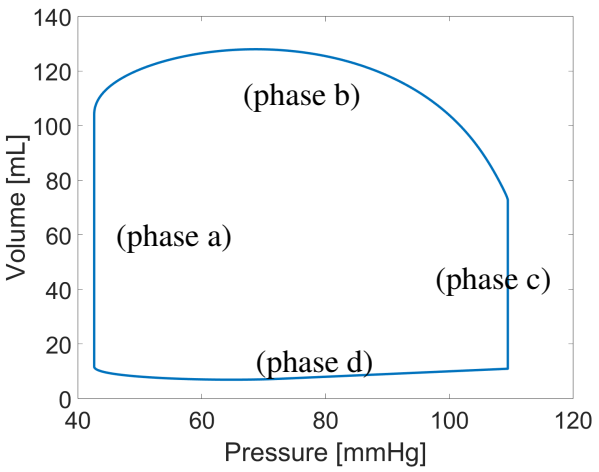

Figure 3. P-V loop simulated *via* the Eye2Heart model.

The model predictions for key ocular biomarkers are tested against quantitative indicators of blood flow in the CRA and CRV (Figure 4).

Key metrics include the following:

- CRA Mean Blood Flow (BF): average blood flow in the CRA, compared to clinical measurements.
- CRA Peak Systolic and End-Diastolic BF: Maximum and minimum values of CRA BF.
- CRV Mean Blood Flow: Mean blood flow in the CRV, considering different age groups.

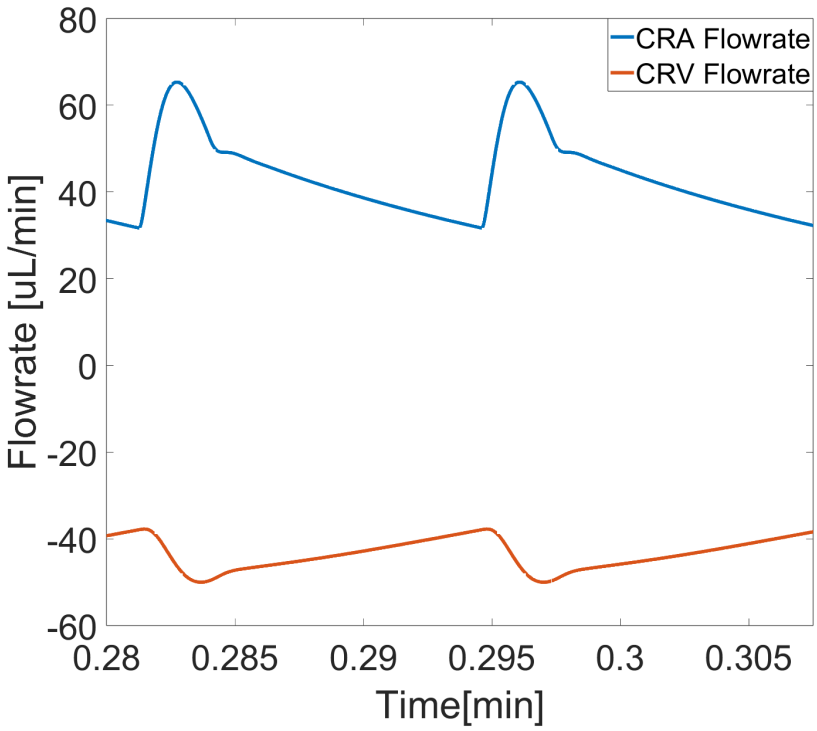

Figure 4. CRA (blue line) and CRV (orange line) blood flows.

- Mean Blood Pressures in the CRA (P_{cra}), retinal arterioles (P_{art}), retinal venules (P_{ven}), and CRV (P_{crv}).

Table 2 presents the model predictions alongside the experimental reference values.

The model shows a strong agreement with clinical data for ocular circulation, particularly CRA and CRV blood flows. The predicted CRA mean flow ($46.56\,\mu l/min$) is consistent with the reported values, with minor deviations likely due to vessel diameter assumptions.

The CRA peak systolic and end-diastolic flows are slightly higher than some measurements, possibly reflecting differences in experimental conditions or systemic pressure assumptions. The CRV flows align well with the literature, thus confirming the model's ability to capture venous return.

Since direct pressure measurements are rarely available in clinical practice, we compared predictions with those from the validated model of [12], thus finding good consistency.

In conclusion, while minor deviations exist, the model successfully replicates cardiovascular and ocular circulation metrics, thus supporting its validity. Refinements in the parameter estimation and integration of additional experimental data could further enhance the predictive accuracy, particularly in capturing inter-individual variability.

3.2. Predictive scenarios

To explore the physiological implications of altered cardiovascular and ocular dynamics, we designed three predictive simulations (Scenarios A, B, and C). Each scenario examines a distinct combination of systemic and local regulatory factors, thereby focusing on how specific parameters influence

Table 2. Experimental data, blood flow. * uses assumption on CRA diameter value of about 160 μm [17, 37].

Description	Unit	Value	Reference	Present work
CRA mean BF	$[\mu l/min]$	40.91	[12]	46.56
	$[\mu l/min]$	38.1 ± 9.1	[17]	
	$[\mu l/min]$	33 ± 9.6	[32]	
CRA peak systolic BF	$[\mu l/min]$	120.6 *	[33]	129.46
	$[\mu l/min]$	122.5 *	[34]	
CRA end diastolic BF	$[\mu l/min]$	30.1 *	[33]	54.76
	$[\mu l/min]$	30 *	[34]	
CRV mean BF	$[\mu l/min]$	64.9 ± 12.8	[35]	43.47
25 - 38 years	$[\mu l/min]$	80 ± 12	[36]	
54 - 58 years	$[\mu l/min]$	73 ± 13	[36]	
CRA Mean Pressure (P_{cra})	[mmHg]	43.92	[12]	44.55
Retinal Arterioles Mean Pressure (P_{art})	[mmHg]	36.09	[12]	35.71
Retinal Venules Mean Pressure (P_{ven})	[mmHg]	22.13	[12]	20.47
CRV Mean Pressure (P_{crv})	[mmHg]	18.84	[12]	17.4

perfusion across the coupled heart-eye system. The two key parameters investigated in this study are the left ventricular compliance (LVc) and the IOP. These were chosen based on their established clinical relevance and their central role in modulating global and local hemodynamics. From a cardiological perspective, the LVc is a proxy for left ventricular contractility and is closely linked, in our modeling, to E_{LS}. Indeed, in our model, E_{LS} is dynamically modulated by the cardiac activation function $a(t)$, as described in Appendix D. Variations in the LVc may reflect pathological changes such as those seen in systolic heart failure, where reduced contractility leads to impaired systemic perfusion [38]. On the other hand, the IOP is a fundamental parameter in ocular physiology and is tightly linked to diseases such as glaucoma. An elevated IOP can impede the ocular blood flow and increase the retinal venous pressure, thus contributing to progressive damage to the optic nerve head (ONH) [1]. Moreover, because the eye is a uniquely accessible site to directly observe the microvasculature, changes in retinal perfusion offer a noninvasive window into systemic vascular health. Prior studies have demonstrated associations between alterations in the retinal vasculature and cardiovascular conditions such as arterial hypertension and coronary heart disease [39].

The formulation of these predictive scenarios is inspired by clinical questions that bridge cardiology and ophthalmology. For instance, Optical Coherence Tomography Angiography (OCTA) studies have shown that patients with chronic systolic heart failure exhibit reduced retinal and ONH flow density compared to healthy individuals. These reductions were found to correlate with the left ventricular

ejection fraction [40]. Such findings suggest that an impaired cardiac function can have measurable consequences on ocular microperfusion, thus motivating our focus on the LVc in particular.

Our simulations aim to test plausible hypotheses that arise from these clinical observations. Specifically, we examine how reductions in the LVc (*i.e.*, diminished contractility) and elevations in the IOP, individually and in combination, affect the perfusion patterns in both the cardiovascular system and the retina. This approach allows us to assess not only the direct hemodynamic consequences but also the interplay between systemic and local regulatory mechanisms. While we do not claim to replicate specific pathologies, the scenarios are constructed to reflect physiologically plausible perturbations that can guide future experimental and clinical investigations.

3.2.1. Simulation A: impact of an increase in IOP on the Eye2Heart model

In this scenario, we investigated the effect of varying the IOP from 15 mmHg to 30 mmHg. This study is motivated by clinical insights which highlight the crucial role of venous circulation and the collapsibility of veins in ocular hemodynamics [41]. Given the challenges associated with directly measuring venous parameters in clinical settings, mathematical modeling provides a valuable tool to infer these values and to gain a deeper understanding of the underlying physiological mechanisms.

As the IOP increases, a marked decrease in the CRA blood flow is observed, thus reflecting the restriction of the vascular supply due to elevated pressure. In contrast, the CRV blood flow increases due to augmented resistance in the venous return pathway (see Figure 5).

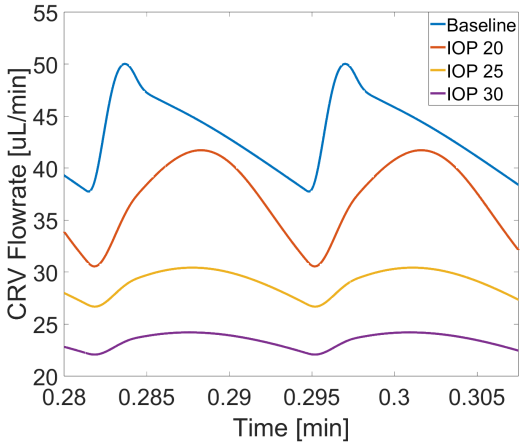

Figure 5. Scenario A: CRV blood flow.

The simulation results, reported in Table 3, indicate a clear trend of decreasing the CRA blood flow and increasing the CRV blood flow as the IOP rises. Despite these variations, the other cardiovascular parameters at a systemic level, such as SP/DP, EDV/ESV, and CO, remain largely unaffected by changes in the IOP, as expected.

Table 3. Scenario A. IOP: Intraocular Pressure.

Output	Unit	IOP = 15 mmHg	IOP = 20 mmHg	IOP = 25 mmHg	IOP = 30 mmHg
SP / DP	[mmHg]	128/69	127/69	127/69	127/69
EDV / ESV	[ml]	113/43	113/43	113/43	113/43
CO	[l/min]	5.26	5.26	5.26	5.26
CRA mean BF	[$\mu l/min$]	46.6	43.6	36.3	30.8
CRV mean BF	[$\mu l/min$]	43.5	40.5	29.1	23.3

3.2.2. Simulation B: effect of left ventricle compliance reduction on the EYE2HEART model.

Simulation B focused on the impact of reducing the LVc, adjusted by 10%, 30%, and 50%. This change was modeled by altering the elastance scaling (ELS) parameter, which reflects the ability of the left ventricle to stretch and contract during the cardiac cycle. This simulation setup builds upon the work of [42], which primarily investigated cardiac dynamics. Here, we extend the analysis to include ocular circulation, thus allowing for a comprehensive assessment of how changes in the LVc influence both systemic and retinal hemodynamics.

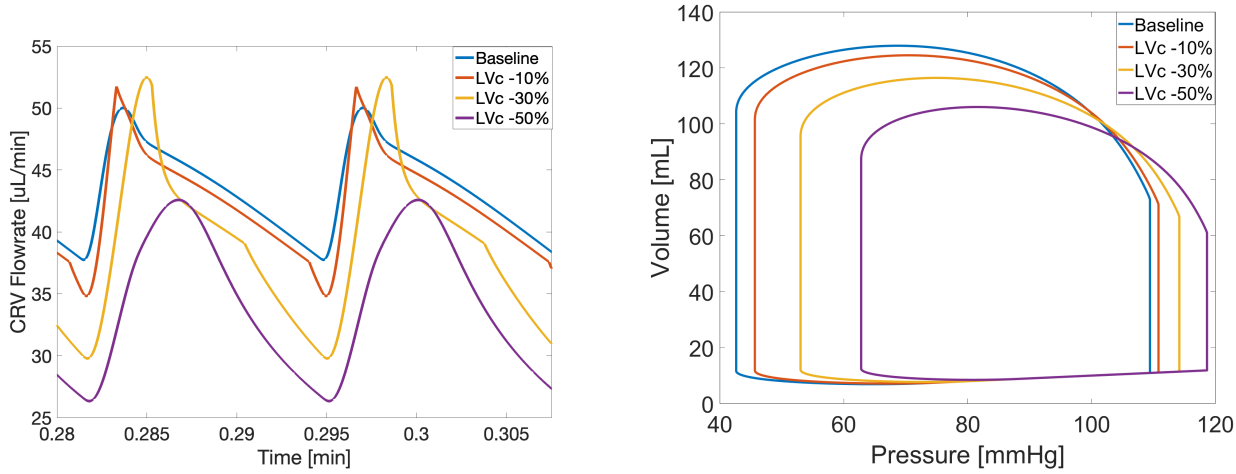

(a) CRV blood flow. **(b)** P-V loop

Figure 6. Scenario B simulation results.

Table 4. Scenario B. LVc: Left Ventricle compliance.

OUTPUT	UNIT	LVC: BASELINE	LVC: -10%	LVC: -30%	LVC: -50%
SP / DP	[mmHg]	128/69	123/69	116/67	107/61
EDV / ESV	$[ml]$	113/43	113/46	114/53	119/62
CO	$[l/min]$	5.26	5.03	4.59	4.24
CRA mean BF	$[\mu l/min]$	46.6	45.6	43.0	38.1
CRV mean BF	$[\mu l/min]$	43.5	43.3	41.1	35.2

The simulation results in Table 4 show a decrease in the SP/DP and CO, as well as an increase in both the EDV and ESV as the LVc is reduced. These changes can be attributed to the decreased ability of the left ventricle to expand and contract effectively when its compliance is reduced. A lower LV compliance leads to less efficient filling and ejection, lowering pressures and cardiac output. At the same time, the reduced compliance causes the ventricle to hold more blood at both the end of diastole and systole, which is reflected in the increase in the EDV and ESV. These results highlight how an impaired ventricular compliance can significantly affect both the pumping efficiency and volume

dynamics of the heart (see Figure 6b).

On the ocular side, changes in the LV compliance also impact the retinal blood flow. As the LVc decreases, there is a reduction in the CRA and CRV blood flows. These changes are more pronounced in the CRA blood flow, which decreases in response to a lower cardiac output. Additionally, the CRV flow (Figure 6a) is affected, especially when the LVc is reduced by 50%. These results suggest that cardiovascular alterations may influence the ocular circulation, thereby reflecting the dependencies between the heart and ocular dynamics.

3.2.3. Simulation C: combined effects of LVc reduction and IOP increase

Finally, Simulation C explores the combined effects of reducing the LVc while simultaneously varying the IOP. Variations in the IOP, similarly to Scenario A, primarily affect the ocular system at a local level, without a significant impact on the overall cardiovascular dynamics. As reported in Table 5, the overall cardiovascular functions - SP/DP, EDV/ESV, and CO, respectively - remain largely unchanged when varying the IOP. This confirms the hypothesis that IOP-related effects are confined to the local ocular circulation, while global system parameters remain stable.

Table 5. Scenario C: simulation results for systemic cardiovascular outputs.

SP/DP [mmHg]	IOP = 15 mmHg	IOP = 20 mmHg	IOP = 25 mmHg	IOP = 30 mmHg
LVc: Baseline	128/69	127/69	127/69	127/69
LVc: -10%	123/69	123/69	123/69	123/69
LVc: -30%	116/67	116/67	116/67	116/67
LVc: -50%	107/61	107/61	107/61	107/61
EDV/ESV [ml]	IOP = 15 mmHg	IOP = 20 mmHg	IOP = 25 mmHg	IOP = 30 mmHg
LVc: Baseline	112.8/42.6	112.8/42.6	112.8/42.6	112.8/42.6
LVc: -10%	112.76/45.7	112.8/45.7	112.8/45.7	112.8/45.7
LVc: -30%	114.2/52.9	114.2/52.9	114.2/52.9	114.2/52.9
LVc: -50%	118.6/62.1	118.6/62.1	118.6/62.1	118.6/62.1
CO [l/min]	IOP = 15 mmHg	IOP = 20 mmHg	IOP = 25 mmHg	IOP = 30 mmHg
LVc: Baseline	5.26	5.26	5.26	5.26
LVc: -10%	5.03	5.03	5.03	5.03
LVc: -30%	4.59	4.59	4.59	4.59
LVc: -50%	4.24	4.24	4.24	4.24

However, the combination of reduced LVc and increased IOP has a marked effect on ocular hemodynamics. For the CRA (top of Table 6), as IOP increases, blood flow decreases in a predictable manner, which is consistent with the vascular resistance caused by elevated pressure. However, the

impact is moderate and does not lead to a dramatic alteration in flow until IOP reaches higher levels (*e.g.*, 30 mmHg). This shows the resilience of the CRA in maintaining blood flow despite increasing IOP.

Table 6. Scenario C: simulation results for ocular circulation outputs.

CRA MEAN BF $[\mu l/min]$	IOP = 15 mmHg	IOP = 20 mmHg	IOP = 25 mmHg	IOP = 30 mmHg
LVc: BASELINE	46.6	43.6	36.3	30.8
LVc: -10%	45.6	42.0	35.0	29.6
LVc: -30%	43.0	38.3	31.8	26.8
LVc: -50%	38.1	33.6	27.8	23.1
CRV MEAN BF $[\mu l/min]$	IOP = 15 mmHg	IOP = 20 mmHg	IOP = 25 mmHg	IOP = 30 mmHg
LVc: BASELINE	43.5	40.5	29.1	23.3
LVc: -10%	43.3	38.8	28.5	23.1
LVc: -30%	41.1	35.0	27.4	22.4
LVc: -50%	35.2	31.7	26.2	21.2

More strikingly, the CRV (bottom of Table 6) shows a pronounced sensitivity to both factors. As the IOP rises, the pressure exerted on the veins increases, and this external pressure can interfere with the venous return, especially when the internal pressure within the veins, driven by cardiovascular dynamics, is lower than the external pressure (IOP). This phenomenon, known as the Starling effect, can cause venous collapse and a reduced blood flow.

For example, at IOP = 25 mmHg, the blood flow in the CRV is noticeably impaired even with a baseline LVc. However, when the LVc is reduced by 50%, the CRV blood flow is significantly compromised even at lower IOP levels (*e.g.*, IOP = 15 mmHg). This drop in blood flow in the CRV under lower IOP conditions suggests that the combination of reduced LVc and IOP increase could be indicative of certain pathologies, such as Normal Tension Glaucoma (NTG), where the vascular flow is impaired despite normal values of the IOP.

This shift in blood flow dynamics highlights the critical interaction between cardiovascular health and ocular pressure in regulating retinal blood flow. Additionally, it points to the potential for these combined factors to serve as biomarkers for ocular conditions such as NTG, where the blood supply to the retina may be compromised despite typical IOP values.

4. Discussions and conclusions

This study introduces the EYE2HEART model, a novel closed-loop framework designed to bridge the gap between cardiovascular and ocular dynamics. By integrating cardiovascular and retinal models, EYE2HEART provides a comprehensive platform to simulate the interconnected functions of these systems. Using a hydraulic-electrical analogy, the model effectively captures the dynamic interactions, thus offering a robust tool that can be adapted for multiple applications, such as studying the impact of

cardiovascular diseases on ocular health and understanding how retinal pathologies are influenced by systemic circulation.

Section 3 presented the validation against clinical and experimental data thereby demonstrating the model's ability to replicate key physiological parameters within acceptable ranges. For the cardiovascular system, parameters such as EDV, ESV, SV, CO, and EF align with clinical values, thus confirming the model's capacity to simulate fundamental cardiac dynamics. Ocular parameters, including CRA and CRV blood flow, also align with experimental data, supporting the model's accuracy in retinal hemodynamics.

Additionally, scenario predictions demonstrate the model's ability to explore the effects of various physiological changes on both ocular and cardiovascular systems. For instance, simulations reveal how variations in the LVc and IOP influence the retinal blood flow and overall cardiovascular function. These predictions highlight the potential of the Eye2Heart model for detailed *in silico* experimentation, thus allowing for the testing of different physiological states and their impact on ocular health and cardiovascular dynamics. In particular, the Eye2Heart model highlights the multi-scale nature of cardiovascular–ocular interactions: systemic cardiac output, pressures, and elastance at the macro-scale directly shape retinal hemodynamics at the micro-scale. This explicit linkage clarifies how even modest variations in central dynamics can manifest as measurable ocular biomarkers.

Beyond *in silico* experimentation, the Eye2Heart model also has a clear translational scope. First, it provides a mechanistic framework to interpret ocular biomarkers within the context of systemic physiology, thus contributing to the emerging field of oculomics. Second, it can be extended toward patient-specific simulations by incorporating individualized parameters, thus opening the way to digital twin applications in ophthalmology and cardiology. Third, it supports hypothesis generation, for instance, on the role of ocular hemodynamics in normal-tension glaucoma or on mechanistic links between heart failure and retinal circulation. It is worth noting that the IOP is routinely measured in clinical practice using tonometry, which facilitates the integration of this model with available patient data.

In terms of clinical applications, the Eye2Heart model holds significant potential for early detection of cardiovascular dysfunction, particularly through a CRA waveform analysis. Previous work, such as that by the group [43], has demonstrated how the analysis of the CRA waveform can yield valuable insights into cardiovascular health. Embedding such a waveform analysis within the Eye2Heart framework, though not yet available in its current implementation, would enable quantitative, model-informed interpretation of ocular signals as surrogates for cardiovascular health, supporting translational applications and the development of noninvasive digital biomarkers.

Nonetheless, certain limitations are acknowledged. Discrepancies such as slight underestimations in the EDV and ESV, as well as deviations in E_{es} and E_a, likely stem from model simplifications, assumptions in pressure-volume relationships, and the exclusion of individual variability. Additionally, the "eye branch" simplification, while computationally efficient, does not fully represent the complexity of non-retinal ocular circulation and represents only a single eye. The model currently assumes a balance between the CRA inflow and the CRV outflow. However, collateral pathways such as the Circle of Zinn–Haller and the cilioretinal artery, present in about half of the population, may alter optic nerve head circulation. These are not captured in the present framework and represent a direction for future refinement. Furthermore, the use of 0D modeling and assumptions regarding parameterization, such as differences between males and females [44], introduces potential limitations in accuracy.

The present version of the model does not include short- and long-term systemic feedbacks such as the arterial baroreflex and the renin–angiotensin–aldosterone system (RAAS), nor ocular autoregulatory responses. These mechanisms are essential to capture homeostatic adaptation across time scales and will be the focus of future extensions. On the ocular side, autoregulation has been investigated in prior modeling work (e.g., [12]), which offers a principled pathway for integration within Eye2Heart . Given the added complexity and parameter burden, we adopt a step-by-step strategy: first establish and validate the coupled hemodynamics, then incrementally incorporate systemic and ocular regulatory loops with dedicated calibration and validation.

Especially in terms of the parameterisation, one of the limitations of the present work is that a full joint calibration of all parameters is currently not feasible due to the absence of a comprehensive dataset simultaneously capturing cardiovascular and ocular measurements. Such a dataset would require the concurrent acquisition of systemic and retinal hemodynamics under standardized protocols and instrumentation, ideally across a large cohort of subjects. Its development would represent a significant advancement to quantitatively assess the interplay between cardiovascular regulation and ocular physiology, both in health and disease.

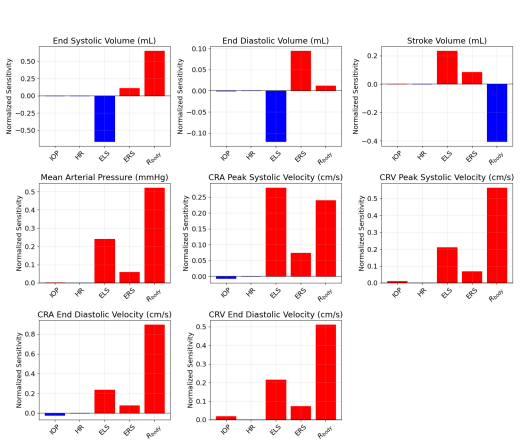

(a) Normalized sensitivities of systemic and ocular outputs to selected parameters of interest.

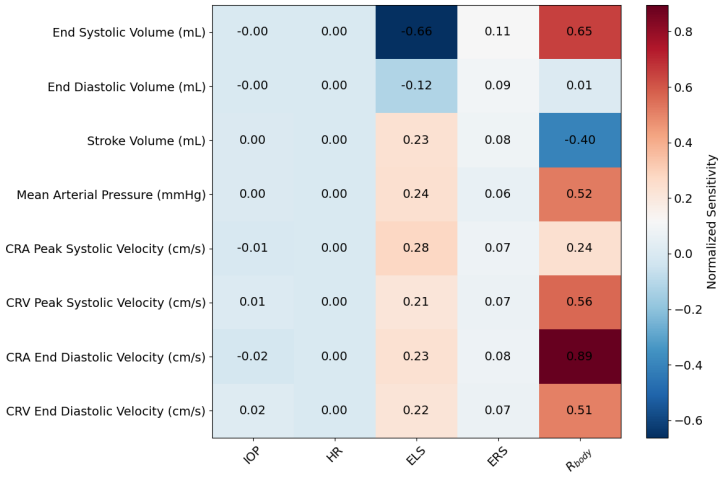

(b) Heatmap summarizing relative parameter influence.

Figure 7. Local sensitivity analysis of the coupled Eye2Heart model.

Despite these limitations, the Eye2Heart model represents a significant advancement in the integrated modeling of cardiovascular and ocular systems. By providing a unified framework, this model offers a valuable tool to explore the complex interactions between these systems and for investigating the potential impact of ocular dynamics on overall cardiovascular health. Future work should focus on refining the model parameters, incorporating individual variability, and expanding the model to include more detailed representations of ocular substructures and both eyes. This expansion would enable the investigation of personalized treatments and their differential effects on each eye. To better account for individual variability, future work should incorporate a systematic sensitivity analysis and uncertainty quantification, as proposed by the group for the ocular system in [45]. Such analyses would allow us to identify the parameters that most strongly influence key systemic and ocular outputs, disentangle macro- and micro-scale interactions, and assess the robustness of the model under different physiological conditions. Beyond improving confidence in the predictions, this step is essential to translate

the model toward clinical applications, where patient-specific variability and parameter uncertainty play a central role. As a first step toward this goal, we performed a preliminary local sensitivity analysis to quantify the influence of selected key parameters on systemic and ocular outputs (Figure 7). The analysis identifies the left-ventricular compliance (ELS) and the peripheral resistance (R_{body}) as the most sensitive parameters across both cardiovascular and ocular variables. Increases in the ELS enhance the SV and MAP, thus reflecting the role of ventricular contractility, whereas a higher R_{body} amplifies the arterial pressure and retinal blood velocities through vascular coupling. Conversely, the IOP primarily affects the ocular hemodynamics with minimal systemic impact. These results are consistent with our previous work on ocular and cardiovascular modeling [11, 45, 46] and reinforce the physiological coherence of the coupled framework. Identifying ELS, R_{body}, and IOP as key determinants highlights parameters that are physiologically meaningful, thus supporting future calibration and validation efforts.

Additionally, future extensions should incorporate biomechanical and electro-chemo-mechanical couplings, to capture how reciprocal interactions between pressure, tissue mechanics, and electrical activity shape patient-specific eye–heart responses. Furthermore, extending the model to include a 4-chamber heart and both eyes would enhance its predictive capabilities, thereby improving its potential clinical applications to diagnose and manage conditions that affect both the eye and the heart.

Importantly, this work aligns with the emerging field of oculomics by providing a mechanistic framework to interpret ocular biomarkers in relation to the cardiac dynamics. Thus, the EYE2HEART model offers a quantitative, physiologically grounded complement to AI-based approaches, thus contributing to the development of explainable digital biomarkers and precision medicine strategies at the intersection of ophthalmology and cardiology.

In conclusion, this study opens new avenues for experimental research investigating the relationship between a patient's visual field deterioration and cardiac health. Understanding these connections could pave the way for new diagnostic approaches that link ocular hemodynamics with systemic cardiovascular conditions. This novel coupling of cardiovascular and retinal circulation models represents a significant step forward in exploring the interdisciplinary relationship between heart function and ocular health, with the potential to improve the diagnostic and therapeutic strategies in both fields.

Acknowledgments

Professor Giovanna Guidoboni has been partially supported by NSF DMS 2108711/2327640, NIH R01EY030851, NIH R01EY034718, and in part by a Challenge Grant award from Research to Prevent Blindness, NY. Professor Alon Harris is supported by NIH grant R01EY034718, NYEE Foundation grants, The Glaucoma Foundation, and in part by a Challenge Grant award from Research to Prevent Blindness, NY. Professor Alon Harris is supported by the Barry Family Center for Ophthalmic Artificial Intelligence & Human Health. The authors are grateful to the American Institute of Mathematics for the support and hospitality during the SQuaRE program.

Use of AI tools declaration

The authors declare they have not used Artificial Intelligence (AI) tools in the creation of this article.

Conflict of interest

Professor Alon Harris would like to disclose that he received remuneration from AdOM, Qlaris, and Cipla for serving as a consultant, and he serves on the board of AdOM, Qlaris and SlitLed. Professor Alon Harris holds an ownership interest in AdOM, Oxymap, Qlaris, SlitLed, and AEYE Health. If you have questions regarding paid relationships that your physician/researcher may have with industry, you are encouraged to talk with your physician/researcher, or check for industry relationships posted on individual faculty pages on our website at http://icahn.mssm.edu/.

References

1. J. Flammer, K. Konieczka, R. M. Bruno, A. Virdis, A. J. Flammer, S. Taddei, The eye and the heart, *Eur. Heart J.*, **34** (2013), 1270–1278. https://doi.org/10.1093/eurheartj/eht023
2. H. Hanssen, L. Streese, W. Vilser, Retinal vessel diameters and function in cardiovascular risk and disease, *Prog. Retin. Eye Res.*, **91** (2022), 101095. https://doi.org/10.1016/j.preteyeres.2022.101095
3. E. L. Michelson, J. Morganroth, C. W. Nichols, H. MacVaugh, Retinal arteriolar changes as an indicator of coronary artery disease, *Arch. Intern. Med.*, **139** (1979), 1139–1141. https://doi.org/10.1001/archinte.1979.03630470051017
4. E. Tedeschi-Reiner, M. Strozzi, B. Skoric, Z. Reiner, Relation of atherosclerotic changes in retinal arteries to the extent of coronary artery disease, *Am. J. Cardiol.*, **96** (2005), 1107–1109. https://doi.org/10.1016/j.amjcard.2005.05.070
5. A. Abdin, A. D. Abdin, G. Merone, W. Aljundi, B. Haring, Y. A. Dail, et al., Cardio-ocular syndrome: Retinal microvascular changes in acutely decompensated heart failure, *Eur. J. Heart Fail.*, **26** (2024), 2421–2430. https://doi.org/10.1002/ejhf.3474
6. Z. Zhu, Y. Wang, Z. Qi, W. Hu, X. Zhang, S. K. Wagner, et al., Oculomics: Current concepts and evidence, *Prog. Retin. Eye Res.*, **101350** (2025). https://doi.org/10.1016/j.preteyeres.2025.101350
7. L. A. Ghenciu, M. Dima, E. R. Stoicescu, R. Iacob, C. Boru, O. A. Hațegan, Retinal imaging-based oculomics: Artificial intelligence as a tool in the diagnosis of cardiovascular and metabolic diseases, *Biomedicines*, **12** (2024), 2150. https://doi.org/10.3390/biomedicines12092150
8. W. Hu, Z. Lin, M. Clark, J. Henwood, X. Shang, R. Chen, et al., Real-world feasibility, accuracy and acceptability of automated retinal photography and AI-based cardiovascular disease risk assessment, *npj Digit. Med.*, **8** (2025), 122. https://doi.org/10.1038/s41746-025-01436-1
9. E. Y. Chew, S. A. Burns, A. G. Abraham, M. F. Bakhoum, J. A. Beckman, T. Y. P. Chui, et al., Standardization and clinical applications of retinal imaging biomarkers for cardiovascular disease, *Nat. Rev. Cardiol.*, **22** (2025), 47–63. https://doi.org/10.1038/s41569-024-01060-8
10. H. T. Caddy, L. J. Kelsey, L. P. Parker, D. J. Green, B. J. Doyle, Modelling large scale artery haemodynamics from the heart to the eye in response to simulated microgravity, *npj Microgravity*, **10** (2024), 7. https://doi.org/10.1038/s41526-024-00348-w
11. G. Guidoboni, L. Sala, M. Enayati, R. Sacco, M. Szopos, J. M. Keller, et al., Cardiovascular function and Ballistocardiogram: A relationship interpreted via mathematical modeling, *IEEE Trans. Biomed. Eng.*, **66** (2019), 2906–2917. https://doi.org/10.1109/tbme.2019.2897952

12. G. Guidoboni, A. Harris, S. Cassani, J. Arciero, B. Siesky, A. Amireskandari, et al., Intraocular pressure, blood pressure, and retinal blood flow autoregulation: A mathematical model to clarify their relationship and clinical relevance, *Invest. Ophthalmol. Vis. Sci.*, **55** (2014), 4105–4118. https://doi.org/10.1167/iovs.13-13611

13. A. C. Guyton, J. E. Hall, Cardiac output, venous return, and their regulation, In *Guyton and Hall Textbook of Medical Physiology*, 14th ed., Elsevier, Philadelphia (2021). https://doi.org/10.1016/b978-1-4160-5451-1.00020-7

14. K. Kashiwagi, T. Tsumura, N. Iwasaki, S. Tsukahara, Blood flow of the ophthalmic artery in healthy individuals, *Invest. Ophthalmol. Vis. Sci.*, **53** (2012), 6870–6876.

15. A. C. Guyton, T. G. Coleman, H. J. Granger, Circulation: Overall regulation, *Annu. Rev. Physiol.*, **34** (1972), 13–46. https://doi.org/10.1146/annurev.ph.34.030172.000305

16. G. Avanzolini, P. Barbini, A. Cappello, G. Cevenini, CADCS simulation of the closed-loop cardiovascular system, *Int. J. Biomed. Comput.*, **22** (1988), 39–49. https://doi.org/10.1016/0020-7101(88)90006-2

17. G. T. Dorner, E. Polska, G. Garhöfer, C. Zawinka, B. Frank, L. Schmetterer, Calculation of the diameter of the central retinal artery from noninvasive measurements in humans, *Curr. Eye Res.*, **25** (2002), 341–345. https://doi.org/10.1076/ceyr.25.6.341.14231

18. L. F. Shampine, M. W. Reichelt, J. A. Kierzenka, Solving index-1 DAEs in MATLAB and Simulink, *SIAM Rev.*, **41** (1999), 538–552. https://doi.org/10.1137/s003614459933425x

19. A. M. Maceira, S. K. Prasad, M. Khan, D. J. Pennell, Normalized left ventricular systolic and diastolic function by steady state free precession cardiovascular magnetic resonance, *J. Cardiovasc. Magn. Reson.*, **8** (2006), 417–426. https://doi.org/10.1080/10976640600572889

20. A.M. Maceira, S. K. Prasad, M. Khan, D. J. Pennell, Reference right ventricular systolic and diastolic function normalized to age, gender and body surface area from steady-state free precession cardiovascular magnetic resonance, *Eur. Heart J.*, **27** (2006), 2879–2888. https://doi.org/10.1093/eurheartj/ehl336

21. J. Sandstede, C. Lipke, M. Beer, S. Hofmann, T. Pabst, W. Kenn, et al., Age- and gender-specific differences in left and right ventricular cardiac function and mass determined by cine magnetic resonance imaging, *Eur. Radiol.*, **10** (2000), 438–442. https://doi.org/10.1007/s003300050072

22. M. S. Maurer, D. Burkhoff, L. P. Fried, J. Gottdiener, D. L. King, D. W. Kitzman, Ventricular Structure and Function in Hypertensive Participants With Heart Failure and a Normal Ejection Fraction, *J. Am. Coll. Cardiol.*, **49** (2007), 972–981. https://doi.org/10.1016/j.jacc.2006.10.061

23. Edwards Lifesciences, Normal hemodynamic parameters and laboratory values, 2014.

24. M. M. Gruca, J. A. Slivnick, A. Singh, J. I. Cotella, V. Subashchandran, D. Prabhu, et al., Noninvasive assessment of left ventricular end-diastolic pressure using machine learning–derived phasic left atrial strain, *Eur. Heart J. Cardiovasc. Imaging*, **25** (2024), 18–26. https://doi.org/10.1093/ehjci/jead231

25. L. Manzi, L. Sperandeo, I. Forzano, D. S. Castiello, D. Florimonte, R. Paolillo, et al., Contemporary evidence and practice on right heart catheterization in patients with acute or chronic heart failure, *Diagnostics*, **14** (2024), 136. https://doi.org/10.3390/diagnostics14020136

26. G. de Simone, R. B. Devereux, S. R. Daniels, G. Mureddu, M. J. Roman, T. R. Kimball, et al., Stroke volume and cardiac output in normotensive children and adults, *Circulation*, **95** (1997), 1837–1843. https://doi.org/10.1161/01.cir.95.7.1837

27. M. M. Redfield, S. J. Jacobsen, B. A. Borlaug, R. J. Rodeheffer, D. A. Kass, Age- and gender-related ventricular-vascular stiffening, *Circulation*, **112** (2005), 2254–2262. https://doi.org/10.1161/circulationaha.105.541078

28. I. Singh, R. K. F. Oliveira, P. M. Heerdt, R. Pari, D. M. Systrom, A. B. Waxman, Sex-related differences in dynamic right ventricular-pulmonary vascular coupling in heart failure with preserved ejection fraction, *Chest*, **159** (2021), 2402–2416. https://doi.org/10.1016/j.chest.2020.12.028

29. H. D. Sesso, M. J. Stampfer, B. Rosner, C. H. Hennekens, J. M. Gaziano, J. E. Manson, et al., Systolic and diastolic blood pressure, pulse pressure, and mean arterial pressure as predictors of cardiovascular disease risk in men, *Hypertension*, **36** (2000), 801–807. https://doi.org/10.1161/01.hyp.36.5.801

30. J. E. Lock, Cardiac catheterization, In: J. F. Keane, J. E. Lock, D. C. Fyler (eds.), *Nadas' Pediatric Cardiology*, 2nd ed., WB Saunders, Philadelphia (2006), 213–250. https://doi.org/10.1016/b978-1-4160-2390-6.50019-2

31. R. Klabunde, Cardiovascular physiology concepts, Lippincott Williams & Wilkins, 2011.

32. C. E. Riva, G. T. Feke, B. Eberli, V. Benary, Bidirectional LDV system for absolute measurement of blood speed in retinal vessels, *Appl. Opt.*, **18** (1979), 2301–2306. https://doi.org/10.1364/ao.18.002301

33. A. Harris, K. Joos, M. Kay, D. Evans, R. Shetty, W. E. Sponsel, et al., Acute IOP elevation with scleral suction: Effects on retrobulbar haemodynamics, *Br. J. Ophthalmol.*, **80** (1996), 1055–1059. https://doi.org/10.1136/bjo.80.12.1055

34. L. Julien, S. Bonnin, M. Paques, J.-M. Fullana, One-dimensional modeling of microvascular hemodynamics in the retina using multimodal imaging, *Phys. Fluids*, **35** (2023), 061901. https://doi.org/10.1063/5.0152499

35. J. P. S. Garcia Jr., P. T. Garcia, R. B. Rosen, Retinal blood flow in the normal human eye using the Canon laser blood flowmeter, *Ophthalm. Res.*, **34** (2002), 295–299. https://doi.org/10.1159/000065600

36. G. T. Feke, C. E. Riva, Laser Doppler measurements of blood velocity in human retinal vessels, *J. Opt. Soc. Am.*, **68** (1978), 526–531. https://doi.org/10.1364/josa.68.000526

37. K. E. Lee, B. E. K. Klein, R. Klein, S. M. Meuer, Association of retinal vessel caliber to optic disc and cup diameters, *Invest. Ophthalmol. Vis. Sci.*, **48** (2007), 63–67. https://doi.org/10.1167/iovs.05-1203

38. S. Hsu, J. C. Fang, B. A. Borlaug, Hemodynamics for the heart failure clinician: a state-of-the-art review, *J. Card. Fail.*, **28** (2022), 133–148. https://doi.org/10.1016/j.cardfail.2021.07.012

39. B. R. McClintic, J. I. McClintic, J. D. Bisognano, R. C. Block, The relationship between retinal microvascular abnormalities and coronary heart disease: A review, *Am. J. Med.*, **123** (2010), 374. https://doi.org/10.1016/j.amjmed.2009.05.030

40. M. Alnawaiseh, F. Eckardt, N. Mihailovic, G. Frommeyer, R. Diener, F. Rosenberger, et al., Ocular perfusion in patients with reduced left ventricular ejection fraction measured by optical coherence tomography angiography, *Graefes Arch. Clin. Exp. Ophthalmol.*, **259** (2021), 3605–3611. https://doi.org/10.1007/s00417-021-05253-6

41. R. Rai, G. Guidoboni, C. K. Wikle, F. Topouzis, B. Siesky, A. V. Vercellin, et al., Retinal venous vulnerability in primary open angle glaucoma: The combined effects of intraocular pressure and blood pressure with application to the Thessaloniki eye study, *La Matematica*, (2024), 1–18. https://doi.org/10.1007/s44007-024-00144-8

42. M. Zaid, L. Sala, J. R. Ivey, D. L. Tharp, C. M. Mueller, P. K. Thorne, et al., Mechanism-driven modeling to aid non-invasive monitoring of cardiac function via ballistocardiography, *Front. Med. Technol.*, **4** (2022), 788264. https://doi.org/10.3389/fmedt.2022.788264

43. L. Sala, K. Lyons, G. Guidoboni, A. Harris, M. Szopos, S. Lapin, Analysis of waveform parameters in the retinal vasculature via mathematical modeling and data analytics methods, *La Matematica*, **3** (2024), 1297–1319. https://doi.org/10.1007/s44007-024-00137-7

44. M. Zaid, L. Sala, L. Despins, D. Heise, M. Popescu, M. Skubic, et al., Cardiovascular sex-differences: Insights via physiology-based modeling and potential for noninvasive sensing via ballistocardiography, *Front. Cardiovasc. Med.*, **10** (2023), 1215958. https://doi.org/10.3389/fcvm.2023.1215958

45. C. Prud'homme, L. Sala, M. Szopos, Uncertainty propagation and sensitivity analysis: Results from the Ocular Mathematical Virtual Simulator,, *Math. Biosci. Eng.*, **18** (2021), 2010–2032. https://doi.org/10.3934/mbe.2021105

46. N. M. Marazzi, G. Guidoboni, M. Zaid, L. Sala, S. Ahmad, L. Despins, et al., Combining physiology-based modeling and evolutionary algorithms for personalized, noninvasive cardiovascular assessment based on electrocardiography and ballistocardiography, *Front. Physiol.*, **12** (2022), 739035. https://doi.org/10.3389/fphys.2021.739035

A. Model state variables

Table 7. Summary of model state variables and their initial conditions. CRA=Central Retinal Artery; CRV=Central Retinal Vein.

Variable	Description	Initial condition	Units	Reference
Cardiovascular				
P_{aorta}	aortic pressure	90.1	mmHg	[16]
P_{body}	body pressure	70.5	mmHg	[16]
P_{VC}	vena cava pressure	3.32	mmHg	[16]
P_{PA}	pulmonary artery pressure	13.4	mmHg	[16]
P_{lungs}	lungs pressure	13.3	mmHg	[16]
P_{PV}	pulmonary vein pressure	11.2	mmHg	[16]
Q_{aorta}	aortic flow rate	8.89	ml/s	[16]
Q_{body}	body flow rate	67.3	ml/s	[16]
Q_{lungs}	lungs flow rate	0.78	ml/s	[16]
Q_{PV}	pulmonary vein flow rate	23.8	ml/s	[16]
V_{RV}	vena cava volume	105	ml	[16]
V_{LV}	left ventricle volume	112	ml	[16]
Eye-Heart Coupling				

$P_{aorta2eye,1}$	aorta-to-eye pressure	80.25	mmHg	This work
P_{CRAin}	pre-laminar CRA pressure	70.2	mmHg	This work
P_{CRVout}	post-laminar CRV pressure	8.57	mmHg	This work
P_{eye}	eye pressure	65.5	mmHg	This work
$P_{eye2vc,2}$	eye-to-vena cava pressure	4.52	mmHg	This work
Q_{eye2vc}	eye-to-vena-cava flow rate	0.15	ml/s	This work
$Q_{aorta2eye}$	aorta-to-eye flow rate	0.15	ml/s	This work
Ocular Circulation				
$P_{CRA,1}$	CRA pressure	43.5	mmHg	[12]
P_{art}	arteriole pressure	35.5	mmHg	[12]
P_{ven}	venule pressure	21.8	mmHg	[12]
$P_{CRV,2}$	CRV pressure	18.9	mmHg	[12]

B. Model parameters

Table 8. Summary of model parameters.
CRA=Central Retinal Artery; CRV=Central Retinal Vein.

Symbol	Description	Value	Units	Reference
Cardiovascular system				
$R_{aorta,1}$	aortic resistance	$3.751 \cdot 10^{-3}$	mmHg s / ml	[16]
$R_{aorta,2}$	aortic resistance	$6.93 \cdot 10^{-2}$	mmHg s / ml	This work
R_{body}	body resistance	1.0	mmHg s / ml	[16]
R_{vc}	vena cava resistance	$3.751 \cdot 10^{-3}$	mmHg s / ml	[16]
R_{pa}	pulmonary artery resistance	$3.751 \cdot 10^{-3}$	mmHg s / ml	[16]
$R_{lungs,1}$	lungs resistance	$3.376 \cdot 10^{-2}$	mmHg s / ml	[16]
$R_{lungs,2}$	lungs resistance	0.1013	mmHg s / ml	[16]
R_{pv}	pulmonary vein resistance	$3.751 \cdot 10^{-3}$	mmHg s / ml	[16]
C_{aorta}	aortic compliance	0.22	ml / mmHg	[16]
C_{body}	body compliance	1.46	ml / mmHg	[16]
C_{vc}	vena cava compliance	20.0	ml / mmHg	[16]
C_{pa}	pulmonary artery compliance	$9.0 \cdot 10^{-2}$	ml / mmHg	[16]
C_{lungs}	lungs capacitance	2.67	ml / mmHg	[16]
C_{pv}	pulmonary vein capacitance	46.7	ml / mmHg	[16]
L_{aorta}	aortic fluid inertance	$8.25 \cdot 10^{-4}$	mmHg s^2 / ml	[16]
L_{body}	body fluid inertance	$3.6 \cdot 10^{-3}$	mmHg s^2 / ml	[16]
L_{lungs}	lungs fluid inertance	$7.5 \cdot 10^{-4}$	mmHg s^2 / ml	[16]
L_{pv}	pulmonary vein fluid inertance	$3.08 \cdot 10^{-3}$	mmHg s^2 / ml	[16]
Heart system				
R_{LV}	left ventricle resistance	$8.0 \cdot 10^{-3}$	mmHg s / ml	[16]
R_{RV}	right ventricle resistance	$1.75 \cdot 10^{-2}$	mmHg s / ml	[16]
U_{L0}	left ventricle isovolumic pressure	50.0	mmHg	[16]
E_{LD}	left ventricle diastolic elastance	0.1	mmHg / ml	[16]
E_{LS}	left ventricle systolic elastance	1.375	mmHg / ml	[16]
U_{R0}	right ventricle isovolumic pressure	24.0	mmHg	[16]
E_{RD}	right ventricle diastolic elastance	$3.0 \cdot 10^{-2}$	mmHg / ml	[16]
E_{RS}	right ventricle systolic elastance	0.3288	mmHg / ml	[16]
Ocular hemodynamics				
IOP	intraocular pressure	15	mmHg	[12]
$R_{cra,1a}$	pre-laminar CRA resistance	$2.68 \cdot 10^{4}$	mmHg s / ml	[12]
$R_{cra,1b}$	pre-laminar CRA resistance	$4.3 \cdot 10^{3}$	mmHg s / ml	[12]
$R_{art,1}$	retinal arterioles resistance	$6.0 \cdot 10^{3}$	mmHg s / ml	[12]
$R_{art,2}$	retinal arterioles resistance	$6.0 \cdot 10^{3}$	mmHg s / ml	[12]
$R_{cap,1}$	retinal capillaries resistance	$5.68 \cdot 10^{3}$	mmHg s / ml	[12]
$R_{cap,2}$	retinal capillaries resistance	$5.68 \cdot 10^{3}$	mmHg s / ml	[12]
$R_{crv,2a}$	post-laminar CRV resistance	$1.35 \cdot 10^{3}$	mmHg s / ml	[12]

$R_{crv,2b}$	post-laminar CRV resistance	$22.09 \cdot 10^3$	mmHg s / ml	[12]
$K_{l_{cra,2a}}$	CRA nonlinear resistance parameter	58.223	[-]	[12]
$K_{l_{cra,2b}}$	CRA nonlinear resistance parameter	58.223	[-]	[12]
$K_{P_{cra,2a}}$	CRA nonlinear resistance parameter	23.0894	mmHg	[12]
$K_{P_{cra,2b}}$	CRA nonlinear resistance parameter	23.0894	mmHg	[12]
$k_{0_{cra,2a}}$	CRA nonlinear resistance parameter	0.005115	[-]	[12]
$k_{0_{cra,2b}}$	CRA nonlinear resistance parameter	0.001023	[-]	[12]
$K_{l_{crv,1a}}$	CRV nonlinear resistance parameter	$1.48425 \cdot 10^3$	[-]	[12]
$K_{l_{crv,1b}}$	CRV nonlinear resistance parameter	$1.48425 \cdot 10^3$	[-]	[12]
$K_{P_{crv,1a}}$	CRV nonlinear resistance parameter	0.358774	mmHg	[12]
$K_{P_{crv,1b}}$	CRV nonlinear resistance parameter	0.358774	mmHg	[12]
$k_{0_{crv,1a}}$	CRV nonlinear resistance parameter	0.00324	[-]	[12]
$k_{0_{crv,1b}}$	CRV nonlinear resistance parameter	0.0162	[-]	[12]
$K_{l_{ven,1}}$	retinal venules nonlinear resistance parameter	$1.2 \cdot 10^3$	[-]	[12]
$K_{l_{ven,2}}$	retinal venules nonlinear resistance parameter	$1.2 \cdot 10^3$	[-]	[12]
$K_{p_{ven,1}}$	retinal venules nonlinear resistance parameter	0.0543	mmHg	[12]
$K_{p_{ven,2}}$	retinal venules nonlinear resistance parameter	0.0543	mmHg	[12]
$k_{0_{ven,1}}$	retinal venules nonlinear resistance parameter	$2.8025 \cdot 10^{-4}$	[-]	[12]
$k_{0_{ven,2}}$	retinal venules nonlinear resistance parameter	$2.8025 \cdot 10^{-4}$	[-]	[12]
$C_{cra,1}$	CRA compliance	$7.22 \cdot 10^{-7}$	ml / mmHg	[12]
C_{art}	retinal arterioles compliance	$7.53 \cdot 10^{-7}$	ml / mmHg	[12]
C_{ven}	retinal venules compliance	$1.67 \cdot 10^{-5}$	ml / mmHg	[12]
$C_{crv,2}$	CRV compliance	$1.07 \cdot 10^{-5}$	ml / mmHg	[12]
Cardiovascular - ocular connection				
$R_{aorta2eye,1}$	aorta-to-eye resistance	55.062	mmHg s / ml	This work
$R_{aorta2eye,2}$	aorta-to-eye resistance	55.062	mmHg s / ml	This work
$R_{cra,in,1}$	pre-laminar CRA resistance	5254.828	mmHg s / ml	This work
$R_{cra,in,2}$	pre-laminar CRA resistance	5254.828	mmHg s / ml	This work
$R_{crv,out,1}$	pre-laminar CRV resistance	16331.607	mmHg s / ml	This work
$R_{crv,out,2}$	pre-laminar CRV resistance	16331.607	mmHg s / ml	This work
$R_{eye2vc,1}$	aorta-to-vena cava resistance	4.599	mmHg s / ml	This work
$R_{eye2vc,2}$	aorta-to-vena cava resistance	4.599	mmHg s / ml	This work
$R_{eye,1}$	eye resistance	268.777	mmHg s / ml	This work
$R_{eye,2}$	eye resistance	268.777	mmHg s / ml	This work
$C_{aorta2eye}$	aorta-to-eye compliance	$1.66125 \cdot 10^{-5}$	ml / mmHg	This work
$C_{cra,in}$	pre-laminar CRA compliance	$1.72 \cdot 10^{-5}$	ml / mmHg	This work
C_{eye}	eye compliance	$3.6125 \cdot 10^{-6}$	ml / mmHg	This work
$C_{crv,out}$	pre-laminar CRV compliance	$1.6125 \cdot 10^{-4}$	ml / mmHg	This work
C_{eye2vc}	eye-to-vena cava compliance	$6.58 \cdot 10^{-8}$	ml / mmHg	This work
$L_{aorta2eye}$	aorta-to-eye fluid inertance	0.0343	mmHg s^2 / ml	This work
L_{eye2vc}	eye-to-vena cava fluid inertance	0.0042	mmHg s^2 / ml	This work

C. Model equations

The overall description results in the following set of ODEs, which models the coupling between the eye and heart dynamics. These equations describe the hemodynamics between various compartments, including the aorta, body, lungs, and the eye. The system of equations accounts for pressure and flow rates in the cardiovascular and ocular systems, thereby considering factors such as resistance, compliance, and inductance in each compartment. We gather the following equations which govern the overall dynamics of the coupled system:

$$\frac{dP_{aorta}}{dt} = \frac{1}{C_{aorta}} \left(\frac{(P_{LV} - P_{aorta}) S_{aorta}}{R_{LV} - R_{aorta,1}} - Q_{aorta2eye} - Q_{aorta} \right) \tag{C.1}$$

$$\frac{dQ_{aorta}}{dt} = \frac{1}{L_{aorta}}(P_{aorta} - P_{body} - R_{aorta,2}Q_{aorta}) \tag{C.2}$$

$$\frac{dP_{body}}{dt} = \frac{1}{C_{body}}(Q_{aorta} - Q_{body}) \tag{C.3}$$

$$\frac{dQ_{body}}{dt} = \frac{1}{L_{body}}(P_{body} - P_{VC} - R_{body}Q_{body}) \tag{C.4}$$

$$\frac{dP_{VC}}{dt} = \frac{1}{C_{VC}}\left((Q_{body} + Q_{eye2VC}) - \frac{(P_{VC} - P_{RV})S_{VC}}{R_{VC}}\right) \tag{C.5}$$

$$\frac{dV_{RV}}{dt} = \frac{(P_{VC} - P_{PA})S_{VC}}{R_{VC}} - \frac{(P_{RV} - P_{PA})S_{PA}}{R_{RV} + R_{PA}} \tag{C.6}$$

$$\frac{dP_{PA}}{dt} = \frac{1}{C_{PA}}\left(\frac{(P_{RV} - P_{PA})S_{PA}}{R_{RV} + R_{PA}} - Q_{lungs}\right) \tag{C.7}$$

$$\frac{dQ_{lungs}}{dt} = \frac{1}{L_{lungs}}(P_{pa} - P_{lungs} - R_{lungs,1}Q_{lungs}) \tag{C.8}$$

$$\frac{dP_{lungs}}{dt} = \frac{1}{C_{PA}}(Q_{lungs} - Q_{PV}) \tag{C.9}$$

$$\frac{dQ_{PV}}{dt} = \frac{1}{L_{PV}}(P_{lungs} - P_{PV} - R_{lungs}Q_{PV}) \tag{C.10}$$

$$\frac{dP_{PV}}{dt} = \frac{1}{C_{PV}}\left(\frac{(P_{PV} - P_{LV})S_{PV}}{R_{PV}} - Q_{PV}\right) \tag{C.11}$$

$$\frac{dV_{LV}}{dt} = \frac{(P_{PV} - P_{LV})S_{PV}}{R_{PV}} - \frac{(P_{LV} - P_{aorta})S_{aorta}}{R_{LV} + R_{aorta,1}} \tag{C.12}$$

$$\frac{dQ_{aorta2eye}}{dt} = \frac{1}{L_{aorta2eye}}(P_{aorta} - P_{aorta2eye} - R_{aorta2eye,1}Q_{aorta2eye}) \tag{C.13}$$

$$\frac{dP_{aorta2eye,1}}{dt} = \frac{1}{C_{aorta2eye}}\left(Q_{aorta2eye} - \frac{P_{aorta2eye,1} - P_{aorta2eye,2}}{R_{aorta2eye,2}}\right) \tag{C.14}$$

$$\frac{dP_{eye}}{dt} = \frac{1}{C_{eye}}\left(\frac{P_{aorta2eye,2} - P_{eye}}{R_{eye,1}} - \frac{P_{eye} - P_{eye2VC}}{R_{eye,2}}\right) \tag{C.15}$$

$$\frac{dP_{CRAin}}{dt} = \frac{1}{C_{CRAin}}\left(\frac{P_{aorta2eye,2} - P_{CRAin}}{R_{CRAin,1}} - \frac{P_{CRAin} - P_{CRA,1}}{R_{CRAin,2} + R_{CRA,1a}}\right) \tag{C.16}$$

$$\frac{dP_{CRA,1}}{dt} = \frac{1}{C_{CRA,1}}\left(\frac{P_{CRAin} - P_{CRA,1}}{R_{CRAin,2} + R_{CRA,1a}} - \frac{P_{CRA,1} - P_{art}}{R_{CRA,1b} + R_{CRA,2a} + R_{CRA,2b} + R_{art,1}}\right) \tag{C.17}$$

$$\frac{dP_{art}}{dt} = \frac{1}{C_{art}}\left(\frac{P_{CRA,1} - P_{art}}{R_{CRA,1b} + R_{CRA,2a} + R_{CRA,2b} + R_{art,1}} - \frac{P_{art} - P_{ven}}{R_{art,2} + R_{cap,1} + R_{cap,2} + R_{ven,1}}\right) \tag{C.18}$$

$$\frac{dP_{ven}}{dt} = \frac{1}{C_{ven}}\left(\frac{P_{art} - P_{ven}}{R_{art,1} + R_{cap,1} + R_{cap,2} + R_{ven,1}} - \frac{P_{ven} - P_{CRV,2}}{R_{ven,2} + R_{CRV,1a} + R_{CRV,1b} + R_{CRV,2a}}\right) \tag{C.19}$$

$$\frac{dP_{CRV,2}}{dt} = \frac{1}{C_{CRV,1}}\left(\frac{P_{ven} - P_{CRV,2}}{R_{ven,2} + R_{CRV,1a} + R_{CRV,1b} + R_{CRV,2a}} - \frac{P_{CRV,2} - P_{CRVout}}{R_{CRV,2b} + R_{CRVout,1}}\right) \tag{C.20}$$

$$\frac{dP_{CRVout}}{dt} = \frac{1}{C_{CRVout}}\left(\frac{P_{CRV,2} - P_{CRVout}}{R_{CRV,2b} + R_{CRVout,1}} - \frac{P_{CRVout} - P_{eye2VC,1}}{R_{CRVout,2}}\right) \tag{C.21}$$

$$\frac{dP_{eye2VC}}{dt} = \frac{1}{C_{eye2VC}}\left(\frac{P_{eye2VC,1} - P_{eye2VC,2}}{R_{eye2VC,1}} - Q_{eye2VC}\right) \tag{C.22}$$

$$\frac{dQ_{eye2VC}}{dt} = \frac{1}{L_{eye2VC}}(P_{eye2VC,2} - P_{vc} - R_{eye2VC,2}Q_{eye2VC}) \tag{C.23}$$

where all the state variables are defined in Table 7. Valve states S_i with $i = aorta, PV, PA, VC$ represent the valve opening or closure, depending on the local pressure gradients, thus controlling the direction and timing of blood flow between compartments.

D. Nonlinear Model Equations

This appendix reports the full mathematical expressions used in the model for nonlinear resistances and cardiac activation functions. The nonlinear resistances in the retinal vasculature and the time-varying elastance of the heart are central to capturing the effects of the IOP and the cardiac dynamics. These equations are taken from [12] and [11], and are reproduced here for completeness.

D.1. Nonlinear Resistances in Retinal Circulation

The resistances in the CRA, denoted as $R_{cra,2a}$ and $R_{cra,2b}$, are functions of the transmural pressure difference $\Delta P_{cra} = P_{cra,2} - \text{IOP}$, where $P_{cra,2}$ is the pressure in the CRA segment and the IOP is the intraocular pressure (see Figure 1). They are modeled as follows:

$$R_{\text{cra},i} = \frac{1}{k_{0_{\text{cra},i}}}\left(1 + \frac{\Delta P_{\text{cra}}}{K_{p_{\text{cra,i}}}\, K_{l_{\text{cra},i}}}\right)^{-4}, \quad i \in \{2a, 2b\}. \tag{D.1a}$$

The venous segment includes two nonlinear components: $R_{\text{ven},1}$ and $R_{\text{ven},2}$ for the retinal venules, and $R_{\text{crv},1a}$ and $R_{\text{crv},1b}$ for the CRV. The nonlinearity arises due to the transmural pressure differences, which are defined as follows:

$$\Delta P_{\text{ven}} = P_{\text{ven}} - \text{IOP}, \qquad \Delta P_{\text{crv}} = P_{\text{crv},1} - \text{IOP}, \text{ respectively.}$$

For the venular segments ($i \in \{1, 2\}$), the resistance is defined as follows:

$$R_{\text{ven},i} = \begin{cases} \dfrac{1}{k_{0_{\text{ven},i}}}\left(1 + \dfrac{\Delta P_{\text{ven}}}{K_{p_{\text{ven,i}}}\, K_{l_{\text{ven,i}}}}\right)^{-4}, & \text{if } \Delta P_{\text{ven}} \geq 0, \\ \dfrac{1}{k_{0_{\text{ven},i}}}\left(1 - \dfrac{\Delta P_{\text{ven}}}{K_{p_{\text{ven,i}}}}\right)^{4/3}, & \text{if } \Delta P_{\text{ven}} < 0. \end{cases} \tag{D.1b}$$

For the CRV segments ($j \in \{1a, 1b\}$), the resistances are defined as follows:

$$R_{\text{crv},i} = \begin{cases} \dfrac{1}{k_{0_{\text{crv},i}}}\left(1 + \dfrac{\Delta P_{\text{crv}}}{K_{p_{\text{crv,i}}}\, K_{l_{\text{crv,i}}}}\right)^{-4}, & \text{if } \Delta P_{\text{crv}} \geq 0, \\ \dfrac{1}{k_{0_{\text{crv},i}}}\left(1 - \dfrac{\Delta P_{\text{crv}}}{K_{p_{\text{crv,i}}}}\right)^{4/3}, & \text{if } \Delta P_{\text{crv}} < 0. \end{cases} \tag{D.1c}$$

D.2. Time-Varying Elastance in the Heart

The time-varying elastance model captures the contraction and relaxation of the left and right ventricles using a periodic activation function $a(t)$. The cardiac cycle duration is as follows:

$$T_c = \frac{60}{\mathrm{HR}}, \qquad T_s = 0.16 + 0.3\, T_c$$

where HR is the heart rate. The activation function is as follows:

$$a(t) = \begin{cases} \dfrac{1}{2}\left(1 - \cos\left(2\pi \dfrac{t \bmod T_c}{T_s}\right)\right), & \text{if } t \bmod T_c < T_s \\ 0, & \text{otherwise} \end{cases} \tag{D.2a}$$

The left and right ventricular pressures are given by the following:

$$P_{\mathrm{LV}}(t) = U_L(t) + E_L(t)\, V_{\mathrm{LV}}(t) \tag{D.2b}$$

$$P_{\mathrm{RV}}(t) = U_R(t) + E_R(t)\, V_{\mathrm{RV}}(t) \tag{D.2c}$$

where:

$$U_L(t) = U_{L0}\, a(t), \qquad E_L(t) = E_{LD} + E_{LS}\, a(t) \tag{D.2d}$$

$$U_R(t) = U_{R0}\, a(t), \qquad E_R(t) = E_{RD} + E_{RS}\, a(t) \tag{D.2e}$$

These expressions capture the pressure-volume dynamics during systole and diastole and are critical for reproducing realistic pulsatile flow patterns in the coupled system [16].